Journal of Materials Chemistry C

Accepted Manuscript

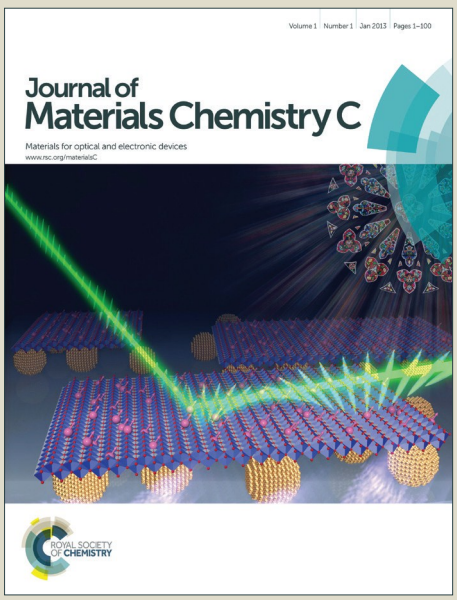

ROYAL SOCIETY OF CHEMISTRY

www.rsc.org/materialsC

Table of Contents Entry

Electronic Supplementary Information for Gold Nanoparticles as an Ultrathin Scattering Layer For Efficient Dye-Sensitized Solar Cells

Lu Zhang and Zhong-Sheng Wang*

Department of Chemistry, Lab of Advanced materials, iChEM (Collaborative Innovation Center of Chemistry for Energy Materials), Fudan University, 2205 Songhu Road, Shanghai 200438, P. R. China

* Corresponding author, E-mail: zs.wang@fudan.edu.cn, Tel/Fax: +86-21-51630345

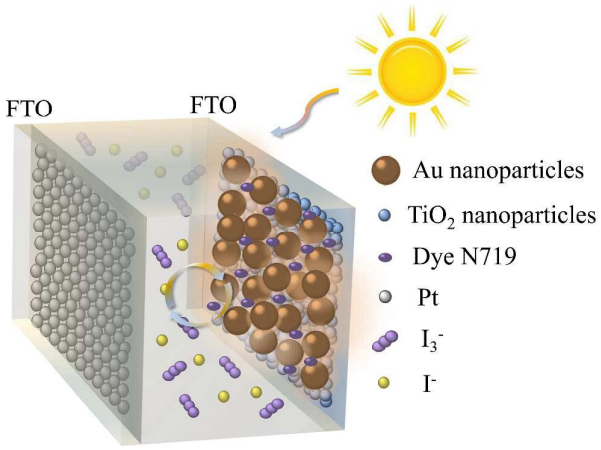

Cite this: DOI: 10.1039/c0xx00000x

www.rsc.org/xxxxxx

ARTICLE TYPE

Gold Nanoparticles as an Ultrathin Scattering Layer For Efficient Dye-Sensitized Solar Cells

Lu Zhang and Zhong-Sheng Wang*

Received (in XXX, XXX) Xth XXXXXXXXX 20XX, Accepted Xth XXXXXXXXX 20XX
DOI: 10.1039/b000000x

Gold nanoparticles with various sizes have been prepared and deposited on top of the TiO_2 film in dye-sensitized solar cells (DSSCs) in order to enhance the light harvesting efficiency. The light scattering effect gradually strengthens as the size of Au nanoparticles increases from 48 to 203 nm. It is impressive that 1 μg cm^{-2} deposition of 203 nm gold nanoparticles on top of the TiO_2 film enhances the light scattering efficiency remarkably, increasing short-circuit photocurrent from 14.37 mA cm^{-2} to 17.81 mA cm^{-2} by 24% and power conversion efficiency from 7.44% to 10.03% by 35%.

Introduction

Dye-sensitized solar cells (DSSCs),[1-4] consisting of a mesoporous TiO_2 film adsorbing a monolayer of dye molecules, a redox electrolyte, and a counter electrode, have attracted great research attention due to the high power conversion efficiency, low cost and easy fabrication. To optimize the performance of DSSCs, scientists have been working on fabricating TiO_2 photoanodes with various nanostructure morphologies[5-8] or different dopants,[9-10] synthesizing novel dye sensitizers[11-13] and developing new electrolytes.[14-15]

In DSSCs, dye as a photon-absorber plays a significant role in absorbing light, generating photo-excited electrons and injecting them into the conduction band of TiO_2 nanocrystalline network. Thus, the light-harvesting efficiency of the dye and the amount of electrons photo-induced from the dye affect the performance of DSSCs significantly. A lot of efforts have been made to design and synthesize new dyes with broad and intense absorption properties. However, it is very difficult for a dye to possess excellent absorption properties and suitable energy levels matching TiO_2 simultaneously. One of the ways to enhance light harvesting is to increase the thickness of the TiO_2 layer so that more dye molecules are available for light harvesting. Nevertheless, this will lead to lower charge collection efficiency, as the electrons have to travel a longer distance to reach the collecting electrode.

Recently, noble metal (e.g. Au, Ag) nanoparticles (NPs) with sizes below 50 nm have been embedded into the TiO_2 network to enhance the light absorption by means of surface plasmon resonance (SPR).[16-25] As the resonant plasmon excitation of gold NPs is able to bring about local electromagnetic field enhancement, the light absorption of surrounding dye molecules can be intensified remarkably. Therefore, significant photocurrent enhancement is achieved due to the SPR effect. However, one big problem of the Au-TiO_2 composite is the significantly decreased dye loading because the gold NPs occupy some part of the TiO_2 surface,[25] which inevitably limits photocurrent generation. To overcome this drawback, we try to deposit small amount of large gold NPs with sizes greater than 50 nm on top of the TiO_2 film rather than in the film, in which the light scattering property of the gold NPs is utilized to enhance light harvesting. In this case, the effective surface area of TiO_2 is decreased negligibly because only the outermost TiO_2 surface is partly occupied by gold NPs, ensuring sufficient dye loading. While the SPR effect of small gold NPs is widely used in DSSCs, the scattering effect of large gold NPs is rarely applied in the photoanode, to the best of our knowledge.

In this study, we prepared a series of gold NPs with sizes of 48 — 203 nm, and deposited them on top of the TiO_2 film as an ultrathin scattering layer. Although TiO_2 scattering NPs have already been used in DSSCs for enhancing light harvesting,[26-28] the increased thickness (e.g. 4 μm) of the active layer inevitably results in a photovoltage loss. As addition of an ultrathin gold NP layer over the TiO_2 film hardly increases the thickness of the active layer, photocurrent can be improved significantly without loss of photovoltage. We have investigated the correlation of scattering properties with the gold particle size and with the photovoltaic performance. It was found that an ultrathin scattering layer of ~203 nm gold NPs (1 μg cm^{-2} deposition) could enhance light harvesting efficiency significantly, resulting in a big improvement of photocurrent and power conversion efficiency.

Experimental

Synthesis of Au Nanoparticles

Synthesis of Au Seeds. The Au nanoparticles were prepared from the chloroauric acid ($HAuCl_4$) precursor using sodium citrate as the reducing agent.[29] 3 mL of 1% w/v $HAuCl_4$ was added to 300 mL of ultra-pure H_2O in a flask, which was heated under stirring. As soon as the solution was boiling, 1.8 mL of 1% w/v sodium citrate solution was added. The flask was removed from heat after stirring for 10 min. The obtained Au nanoparticles were used as seeds for synthesis of larger Au nanoparticles. The

concentration of Au seeds was 0.05 g L^{-1}.

Synthesis of Au nanoparticles with various sizes. Different volume of Au seed solution (800 μL, 400 μL, 200 μL and 50 μL, respectively) was added to a mixture containing 200 μL of 1% w/v $HAuCl_4$ solution and 19 mL of ultra-pure H_2O. 44 μL of 1% w/v sodium citrate was then added to the reaction system, immediately followed by addition of 200 μL hydroquinone (0.03 M) under vigorous stirring at RT. Reduction of $HAuCl_4$ was completed within 20 min. The concentration of Au nanoparticles was 0.05 g L^{-1}.

Fabrication of Photoanodes and DSSCs

TiO_2 films (~12 μm) containing ~ 25 nm nanoparticles[30] were coated on FTO substrates (Fluorine-doped SnO_2, Nippon Sheet Glass Co., Japan, resistance = 14 Ω/sq, transmittance = 90%) with a screen-printing technique. The Au nanoparticles (0.05 g/L, 5 μL) with various sizes were directly dropping on the top of TiO_2 films, corresponding to 1 μg cm^{-2} Au for each TiO_2/Au film. Then the films were sintered at 500 ^oC for 2 h to obtain the TiO_2/Au bilayer photoanodes. Sintered films were then treated with 0.05 M $TiCl_4$ aqueous solution at 70 ^oC for 30 min followed by heating at 450 ^oC for 30 min. These photoanodes were dye-sensitized by immersing them into the solution of cis-di (thiocyanato)-bis(2,2'-bipyridyl-4,4'-dicarboxylate) ruthenium(II) (N719) with a concentration of 0.3 mM in a mixture solvent containing acetonitrile/*tert*-butanol (v/v, 1/1). The redox electrolyte was a mixture of 0.1 M LiI, 0.05 M I_2, 0.6 M 1, 2-dimethyl-3-n-propylimidazolium iodide, and 0.1 M 4-tert-butylpyridine in dehydrated acetonitrile. The counter electrode was Pt-coated FTO. The redox electrolyte was injected into the interspace between working and counter electrodes, and then the DSSCs were sealed with a reported method.[31]

Characterizations

The morphologies and sizes of Au nanoparticles were characterized by field-emitting scanning electron microscope (FESEM, S-4800, Hitachi, Japan). X-ray diffraction (XRD) profiles were determined by an X-ray powder diffractometer (D8 Advance, Bruker) with Cu Kα radiation (λ = 0.154 nm). The film thickness was measured using a step profiler (Veeco Dektak 150, USA). The UV-vis absorption spectra of these samples were analyzed by a Shimadzu UV-2550 UV-Vis spectrometer with an integrating sphere detector. X-Ray photoelectron spectroscopy (XPS) experiments were carried out on a RBD upgraded PHI-5000C ESCA system (Perkin Elmer) with Mg Kα radiation (hv =1253.6 eV). The current density-voltage (*J-V*) curves of the DSSCs were recorded with a Keithley 2420 source meter under illumination of simulated AM 1.5G solar light coming from a Sol3A solar simulator equipped with a 450 W Xe lamp and an AM 1.5G filter. The light intensity was calibrated using a standard Si solar cell (Newport 91150). A black mask with aperture area of 0.2304 cm^2 was used to avoid stray light during measurement. Incident photon-to-current conversion efficiency (IPCE) was measured on a SM-250 system (Bunkoh-keiki, Japan).

Results and discussion

Large Au NPs could be obtained from chemical reduction of $HAuCl_4$ using hydroquinone as a reducing agent in the absence[32-34] and presence[35-36] of Au seeds, respectively. Hydroquinone enables good control over the particle size,[37] which is usually used to prepare Ag[38] and Au[29] NPs via the selective reduction. In this work, Au seeds were obtained from the chemical reduction of $HAuCl_4$ by sodium citrate, and then larger Au NPs were prepared with the seed mediated approach. Fig. 1 shows the SEM images of Au seeds and Au NPs. The diameter of Au seeds estimated from Fig. 1a is ~ 48 nm, while the Au NPs obtained from the seed mediated approach are larger than the Au seeds. The diameters of obtained Au NPs are estimated to be 94 nm (Fig. 1b), 125 nm (Fig. 1c), 162 nm (Fig. 1d) and 203 nm (Fig. 1e). The particle size of gold NPs could be controlled through changing the amount of added Au seeds. The particle size increased with decreasing the amount of Au seeds. It seemed that more Au seeds inhibited the growth of individual particles. These Au NPs were used as the light scattering layer in photoanodes of DSSCs using the smaller Au seeds as the reference.

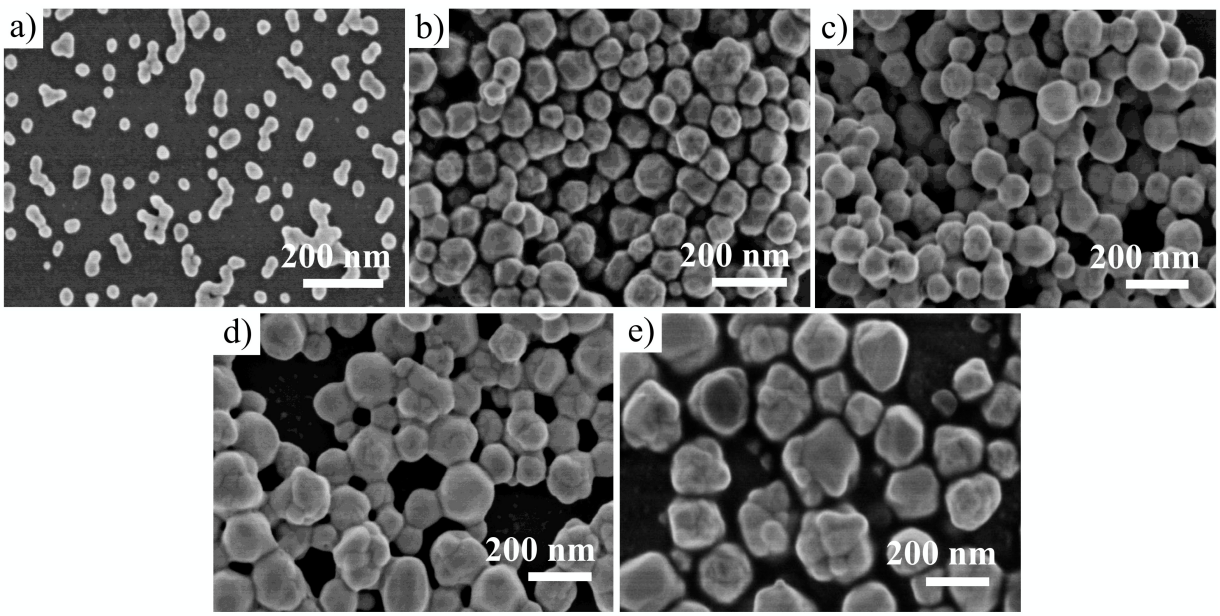

Figure 1. Scanning electron microscopy (SEM) images of the Au nanoparticles: a) ~48 nm; b) ~94 nm; c) ~125 nm; d) ~162 nm; e) ~203 nm.

Cite this: DOI: 10.1039/c0xx00000x

www.rsc.org/xxxxxx

ARTICLE TYPE

X-ray diffraction (XRD) patterns of TiO_2, Au NPs and TiO_2-Au bilayer film are shown in Fig. 2. As seen from curve a in Fig. 2, the peaks at $2\theta = 25.27^o$, 39.85^o, 47.92^o, 53.80^o, 53.88^o, 62.68^o and 75.89^o are respectively assigned to the (101), (004), (200), (105), (211), (204) and (215) lattice planes of TiO_2, which belong to the signals of the anatase TiO_2.[39] As seen from curves b-f in Fig. 2, the Au NPs with various sizes exhibit XRD peaks at the same positions. The peaks at $2\theta = 44.22^o$, 64.64^o and 77.79^o, corresponding to (200), (220) and (311) crystal planes, confirm the fcc structure of Au.[40] As the (200), (220) and (311) XRD peaks for Au NPs are respectively near the (200), (204) and (215) peaks of TiO_2, the TiO_2-Au bilayer film (curve g) shows similar XRD peaks to anatase TiO_2 film. However, the TiO_2-Au bilayer film exhibits higher XRD peak intensity at the four positions for Au (indicated by the triangles in Fig. 2) than the TiO_2 film due to the superposition of XRD peaks. In addition, the typical (101) peak of TiO_2 is also clearly observed in the TiO_2-Au bilayer film (curve g). The XRD data for the TiO_2-Au bilayer film confirms the metallic phase of Au NPs in the electrode.

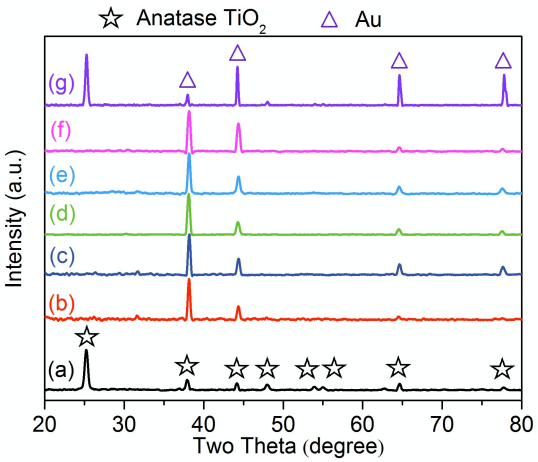

Figure 2. X-ray diffraction (XRD) of (a) TiO_2, (b-f) Au nanoparticles on the glass slide [(b) 48 nm, (c) 94 nm, (d) 125 nm, (e) 162 nm, and (f) 203 nm], and (g) TiO_2/203 nm Au bilayer film.

The UV-vis absorption spectra of Au NPs dispersed in water are shown in Fig. 3a. Shown in the insets of Fig. 3a are the photographs of gold colloids. Table 1 summarizes the color of Au NPs colloid, maximum absorption peak and the peak absorbance. The colors of the gold NPs colloids are related not only to the absorption spectra, but also to other factors such as the quantum color effect, light scattering, refraction and reflection etc..[41, 42] The color of colloidal gold depends on both the size and shape of the particles, as well as the refractive index of the solvent medium.[43] The aggregation of Au NPs of appropriate sizes (d > 3.5 nm) induces inter-particle surface plasmon coupling, resulting in a visible color change from red to blue at nanomolar concentrations.[44] All Au samples show an absorption peak in the visible region, attributed to the plasmon resonance of Au NPs. The plasma band of Au seeds is located at 520 nm. For the Au NPs obtained from the seed mediated approach, the plasma band is shifted to longer wavelength and becomes broader. The characteristic absorption peak red shifts with the particle size, exhibiting a particle size dependence of localized surface plasmon resonance peak of Au NPs.[45] The correlation between maximum absorption peak wavelength and the diameter of Au NPs is plotted in Fig. 3b. When the particle size increases from 48 to 94 nm, the red shift of absorption peak is 41 nm. However, the red shift of absorption peak is less significant with further increasing the particle size, and the total shift is 21 nm when the particle size increases from 94 to 203 nm.

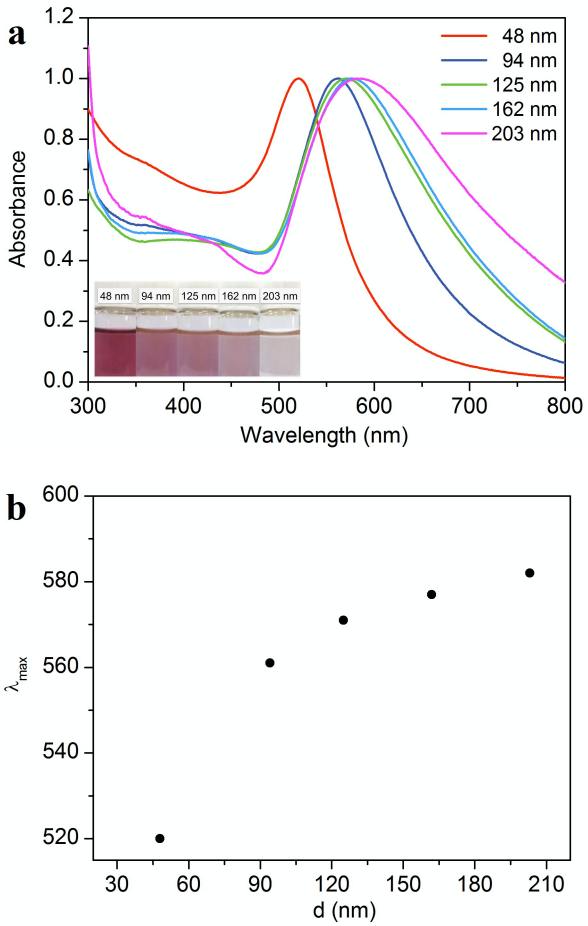

Figure 3. (a) Normalized UV-vis absorption spectra of Au NPs: (1) 48 nm; (2) 94 nm; (3) 125 nm; (4) 162 nm; (5) 203 nm. Inset: photographs of the Au NPs aqueous colloids. (b) Relationship between the maximum absorption wavelength (λ_{max}) and the diameter (d).

Cite this: DOI: 10.1039/c0xx00000x

www.rsc.org/xxxxxx

ARTICLE TYPE

Table 1. Size dependent color, maximum absorption wavelength and absorbance of Au nanoparticles

Average diameter *d* (nm)	Color	λ_{max} (nm)	Absorbance
48	Purple-Red	520	0.92
94	Purple	561	0.75
125	Light Purple	571	0.73
162	Orange	577	0.67
203	Light Orange	582	0.28

The color gradually becomes lighter with increasing the particle size, attributed to the decreased absorbance (Table 1). As the particle size increases, the number of particles decreases for the same mass concentration, which likely accounts for the decreased absorbance. The decrease in peak absorbance means that the plasmonic effect diminishes with the particle size of Au NPs.

To further examine the valence state of Au NPs in the electrode, the X-ray photoelectron spectrum (XPS) of the TiO_2/Au film was carried out. On the basis of the XPS data (Fig. 4), the difference between the Au $4f_{7/2}$ (83.1 eV) and Au $4f_{5/2}$ (86.3 eV) is ~3.2 eV, confirming the metallic phase of Au in the electrode.[46-50] It is noticed that the Au $4f_{7/2}$ of the isolated Au (84.0 eV) shifts to lower energy for the TiO_2-Au film (83.1 eV), which is attributed to the interaction between Au and TiO_2 NPs.

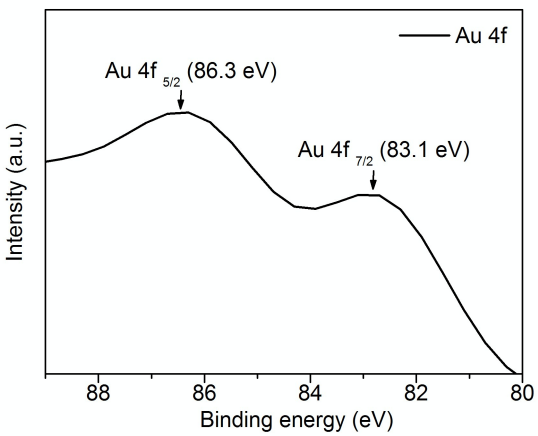

Figure 4. X-Ray photoelectron spectroscopy (XPS) spectrum of the Au (4f) peaks for the TiO_2/Au electrode.

Mie theory predicts that larger metal NPs (diameter > 50 nm) have significant scattering components in their extinction spectra and smaller nanoparticles just have little or no scattering.[51] The scattering effect is dependent on size and refractive index.[51] To evaluate the scattering effect of the Au NPs in the working electrode of DSSCs, the diffused reflection spectra of photoanode films were recorded. Fig. 5a shows the UV-Vis diffused reflection spectra of photoanode films without N719 dye loading. It is evident that the TiO_2/Au films have higher reflectance in the wavelength range of 400-800 nm than the TiO_2 film. The reflectance increases with the size of Au NPs. The results indicate that the 203 nm Au NPs has the highest reflectance among all the films in the wavelength range (400-800 nm). After dye adsorption, although the reflectance of all films decreases (Fig. 5b), which is mainly attributed to the light absorption by the dye molecules, the dye-absorbed TiO_2/Au films still remains a substantially higher reflectance than the dye-loaded TiO_2 film. This means that the TiO_2/Au film has a higher light scattering ability than the TiO_2 film in a real DSSC device. The reflectance also increases with the size of Au NPs for the dye-loaded films.

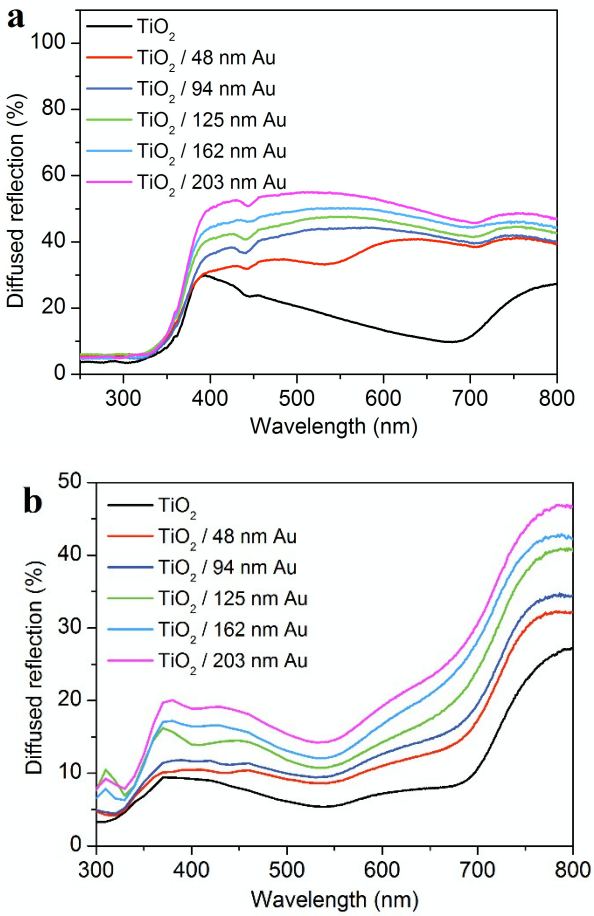

Figure 5. Diffused reflection spectra of the photoanode films (a) without and (b) with the absorbed N719 dye on the FTO substrates.

Current-voltage characteristics of four parallel DSSCs for each photoanode were measured to investigate the effect of top Au layer on the photovoltaic performance. Table 2 lists the

average parameters of the short-circuit current density (J_{sc}), open circuit potential (V_{oc}), fill factor (FF), and power conversion efficiency (η) for each DSSC. The TiO_2 film without a gold scattering layer produces J_{sc} of 14.28 mA cm^{-2}, V_{oc} of 718 mV and FF of 0.72, corresponding to an average η of 7.38%. Upon adding an ultra-thin Au layer, the J_{sc} and V_{oc} increase gradually, but FF hardly changes with the particle size. The increase in V_{oc} with the particle size is the result of the enhanced J_{sc}. As a consequence, the efficiency increases gradually with the particle size of Au NPs.

Table 2. Comparison of the photovoltaic performance parameters of DSSCs sensitized with N719 dye and the adsorbed dye amount on TiO_2

Au size (nm)	V_{oc} (mV)	J_{sc} (mA cm^{-2})	FF	η (%)	Adsorbed dye amount (10^{-8} mol cm^{-2} μm^{-1})
—	718 ± 8	14.28 ± 0.09	0.72 ± 0.01	7.38 ± 0.2	4.1
48 nm	728 ± 5	14.74 ± 0.08	0.72 ± 0.02	7.73 ± 0.5	4.0
94 nm	733 ± 6	15.19 ± 0.17	0.72 ± 0.02	8.02 ± 0.5	3.9
125 nm	735 ± 4	16.18 ± 0.16	0.72 ± 0.02	8.56 ± 0.2	3.9
162 nm	748 ± 3	16.54 ± 0.27	0.73 ± 0.01	9.03 ± 0.2	3.9
203 nm	757 ± 7	17.36 ± 0.11	0.74 ± 0.02	9.72 ± 0.4	3.7

The current-voltage (J-V) characteristics of each individual DSSC are presented in Fig. 6. The DSSC without the top Au layer produces power conversion efficiency of 7.44% (J_{sc} = 14.37 mA cm^{-2}, V_{oc} = 719 mV, FF = 0.72). As can be seen from Fig. 6, the J_{sc} increases upon the deposition of 48 nm Au Seeds and then increases gradually with the particle size of Au NPs. The highest efficiency of 10.03% (J_{sc} = 17.81 mA cm^{-2}, V_{oc} = 761 mV, FF = 0.74) has been achieved with the 203 nm Au NPs, which shows increases in J_{sc} by 24%, in V_{oc} by 5% and in η by 35% as compared to the DSSC without a top Au layer. As the total thickness of the photoanode hardly increases with the top Au layer, as revealed by the top- and side-view SEM images (Fig. S1-5), there is no thickness-induced loss of photovoltage, but an increase in V_{oc} is observed due to the enhanced J_{sc}. With increasing J_{sc}, more electrons are accumulated in the conduction band of TiO_2, which shifts the quasi-Fermi level negatively and thus increases V_{oc}.[25]

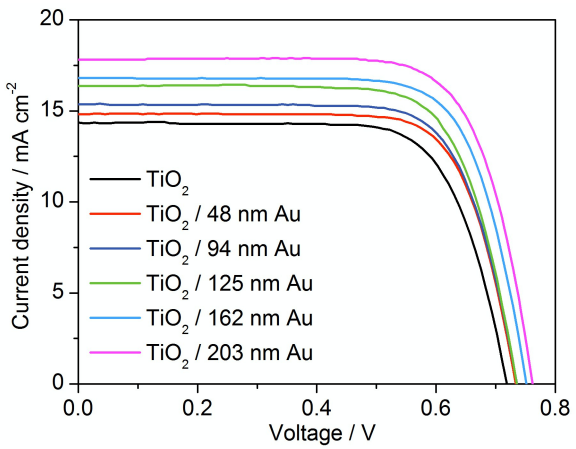

Figure 6. J-V characteristics of the DSSCs based on N719 sensitized TiO_2 and TiO_2/Au electrodes under 100 mW cm^{-2} AM 1.5G illumination.

As electron channels would be formed between TiO_2 and the electrolyte in the presence of Au due to its excellent conductivity, the lifetime of the injected electrons in the conduction band of TiO_2 would decrease, and thus a decrease in V_{oc} would be expected when gold nanoparticles is used as a scattering layer on top of the TiO_2 film. However, we observed an increase in V_{oc}, contrasting to the expectation. As the deposited amount of Au is pretty small (1 μg cm^{-2}), it is possible for a thin TiO_2 layer formed from the $TiCl_4$ treatment to fully protect the Au scattering layer. In this case, electron channels between TiO_2 and the electrolyte cannot be formed because gold nanoparticles are not exposed to the electrolyte. As a consequence, V_{oc} is not reduced. With increasing the amount of Au NPs, since it is difficult for the $TiCl_4$ treatment to completely protect the Au layer, both V_{oc} and J_{sc} decrease gradually (Table S1) due to the electron loss through the electron channels between TiO_2/Au and electrolyte. For instance, 4 μg cm^{-2} of 203 nm Au NPs as a scattering layer yields V_{oc} of 665 mV, J_{sc} of 8.04 mA cm^{-2}, FF of 0.65, corresponding to η of 3.48%. Although more Au NPs is advantageous to get high light scattering efficiency, the formed electron channels decrease the V_{oc}, J_{sc} and η significantly.

Fig. 7 displays the IPCE spectra for the corresponding devices. Upon addition of the top Au layer, the IPCE spectra gradually widen with the particle size of Au along with gradually increased IPCE. The changing tendency of IPCE is consistent with the J_{sc} trend observed in Fig. 6. As compared to the DSSC with TiO_2, the top Au layer (203 nm) increases IPCE from 76% to 90% by 18% at the peak of 540 nm and from 28% to 42% by 50% at 700 nm. The IPCE enhancement caused by the top Au layer is more significant in the longer wavelength region than in the shorter wavelength region, resulting in broadening of the action spectra.

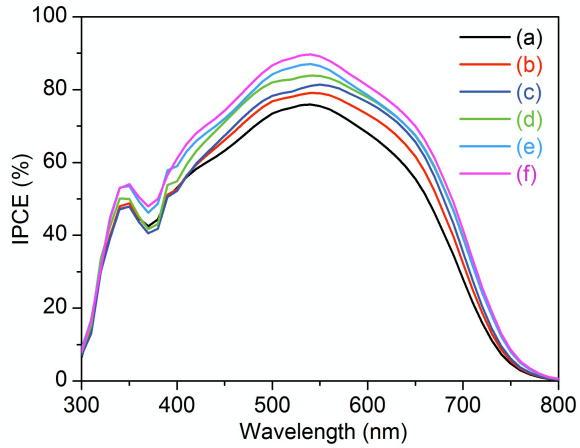

Figure 7. IPCE spectra of DSSC devices. (a) TiO_2 and (b-f) TiO_2/Au films ((b) 48 nm Au, (c) 94 nm Au, (d) 125 nm Au, (e) 162 nm Au, and (f) 203 nm).

The photocurrent is mainly determined by the adsorbed dye amount, the light scattering ability and/or the plasmonic effect of the Au NPs. The dye amount adsorbed on the photoanodes (Table 2), which was measured by the UV-Vis spectra of the dye solutions detached from the dye-loaded films, is similar for these photoanodes. Since the deposited amount of Au NPs on top of TiO_2 layer is pretty small (1 μg cm^{-2}), only the outermost surface of TiO_2 film is partly occupied by the Au NPs, resulting in very small decrease in surface area. Therefore, these TiO_2 films with and without the top Au layer have similar adsorbed dye amount. The effect of dye amount on photocurrent can thus be excluded. It is concluded that the significant increase in photocurrent is attributed to the presence of Au NPs. Plasmonic effect is anticipated for Au NPs, but the plasmon-enhanced light absorption of dye molecules is negligible for these systems. On one hand, the plasmon excitation weakens with the particle size as revealed by the decreased plasma band absorbance shown in Table 1, generating a weak electromagnetic field. On the other hand, only a very small proportion of dye molecules adsorbed on the outermost surface are close to the Au NPs, and most of dye molecules adsorbed onto the inner surface are far away from the Au NPs. The local electromagnetic field caused by the resonant plasmon excitation of Au NPs is just effective for the minority of outermost dye molecules and ineffective for the majority of inner dye molecules due to decaying electromagnetic field. For this reason, the plasmonic effect on the photocurrent enhancement can also be excluded. Based on the above analysis, the main contribution to the photocurrent enhancement coms from the light scattering of top Au layer.

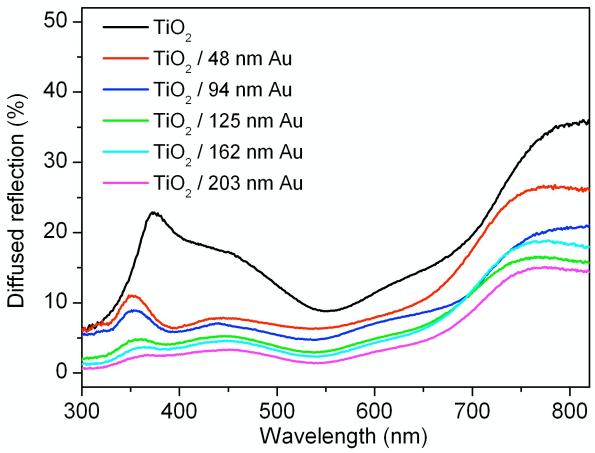

Figure 8. Diffused reflection spectra of DSSC devices.

To further confirm that the increased IPCE is caused by the enhanced adsorption due to the light scattering effect of Au layer, we have measured the reflectance spectra (Fig. 8) of DSSC devices with the incident light passing through the device from the photoanode side. Among various DSSCs, the DSSC without the Au layer has the largest reflectance. Upon introduction of an Au layer, the reflectance decreases gradually with the size of Au NPs. This indicates that the device with higher light scattering effect absorbs more photons, resulting in lower reflectance. As a consequence, the observed increase in IPCE with the particle size of Au is caused by the increased light absorption due to the light scattering effect of Au layer.

When the DSSC is irradiated with the incident light, some photons are absorbed by the dye molecules while some photons particularly in the longer wavelength region transmit through the dye-loaded TiO_2 film. The transmitted photons are reflected back to the dye molecules by the Au NPs so that light-harvesting efficiency is enhanced, resulting in improved IPCE. As more photons with longer wavelength is transmitted through the dye-loaded TiO_2 due to the lower absorption, the enhancement of light harvesting efficiency for the longer wavelength photon is bigger than that for the photons around peak absorption, which increases IPCE in the longer wavelength region more significantly and thus broadens the action spectra. Accordingly, photocurrent is enhanced significantly by the light scattering effect of Au NPs.

Conclusions

We have synthesized Au NPs with various sizes using a seed-mediated approach by controlling the added amount of Au Seeds. It is found that the light-scattering ability increases with the size of Au NPs. Impressively, pretty small loading (1 μg cm^{-2}) of 203 nm Au NPs on top of TiO_2 layer exhibits excellent light scattering effect, improving the light harvesting efficiency remarkably. As a consequence, the short-circuit photocurrent is enhanced from 14.37 mA cm^{-2} to 17.81 mA cm^{-2} by 24% and power conversion efficiency is improved from 7.44% to 10.03% by 35% upon an ultrathin scattering layer of 203 nm Au NPs deposited on top of TiO_2 film. As the ultra-thin scattering Au layer hardly increases the total thickness of photoanode, significant improvement of photocurrent is achieved without loss

of photovoltage. This finding provides a new route for optimizing the photovoltaic performance of DSSCs.

Acknowledgment

This work was financially supported by STCSM (12JC1401500).

References

Department of Chemistry, Lab of Advanced materials, iChEM (Collaborative Innovation Center of Chemistry for Energy Materials), Fudan University, 2205 Songhu Road, Shanghai 200438, P. R. China

* Corresponding author. E-mail: zs.wang@fudan.edu.cn

§ Electronic Supplementary Information (ESI) available: See DOI: 10.1039/b000000x/

1. B. O' Regan and M. Grätzel, *Nature*, 1991, **353**, 737.
2. M. Grätzel, *Nature*, 2001, **414**, 338.
3. M. K. Nazeeruddin, A. Kay, I. Rodicio, R. Humphry-Baker, E. Müller, P. Liska, N. Vlachopoulos and M. Grätzel, *J. Am. Chem. Soc*., 1993, **115**, 6382.
4. N. Koumura, Z.-S. Wang, S. Mori, M. Miyashita, E. Suzuki and K. Hara, *J. Am. Chem. Soc*., 2006, **128**, 14256.
5. G. K. Mor, K. Shankar, M. Paulose, O. K. Varghese and C. A. Grimes, *Nano Lett.*, 2006, **6**, 215.
6. D. Chen, F. Huang, Y.-B. Cheng and R. A. Caruso, *Adv. Mater.*, 2009, **21**, 2206.
7. J. Zhang, Q. Li, S. Li, Y. Wang, C. Ye, P. Ruterana and H. Wang, *J. Power Sources*, 2014, **268**, 941.
8. J. Zhang, S. Li, H. Ding, Q. Li, B. Wang, X. Wang and H. Wang, *J. Power Sources*, 2014, **247**, 807.
9. X. Fang, M. Li, K. Guo, Y. Zhu, Z. Hu, X. Liu, B. Chen and X. Zhao, *Electrochim. Acta*, 2012, **65**, 174.
10. M. R. Mohammadi, A. M. Bakhshayesh, F. Sadri and M. Masroor, *J. Sol-Gel Sci. Technol.*, 2013, **67**, 77.
11. H. Wang, T. Wang, X. Wang, R. Liu, B. Wang, H. Wang, Y. Xu, J. Zhang and J. Duan, *J. Mater. Chem.*, 2012, **22**, 12532.
12. J.-H. Yum, E. Baranoff, S. Wenger, M. K. Nazeeruddin and M. Grätzel, *Energy Environ. Sci.*, 2011, **4**, 842.
13. G.C. Vougioukalakis, A.I. Philippopoulos, T. Stergiopoulos and P. Falaras, *Coord. Chem. Rev.*, 2011, **255**, 2602.
14. S. Ito, S.M. Zakeeruddin, P. Comte, P. Liska, D.B. Kuang and M.Grätzel, *Nat. Photonics*, 2008, **2**, 693.
15. A. Apostolopoulou, M. Vlasiou, P. A. Tziouris, C. Tsiafoulis, A. C. Tsipis, D. Rehder, T. A. Kabanos, A. D. Keramidas and E. Stathatos, *Inorg. Chem.*, 2015, **54**, 3979.
16. H. Dong, Z. Wu, A. El-Shafei, B. Xia, J. Xi, S. Ning, B. Jiao and X. Hou, *J. Mater. Chem. A*, 2015, **3**, 4659.
17. C.-S. Chou, R.-Y. Yang, C.-K. Yeh and Y.-J. Lin, *Powder Technol.*, 2009, **194**, 95.
18. H.-W. Chen, C.-Y. Hong, C.-W. Kung, C.-Y. Mou, K. C. W. Wu and K.-C. Ho, *J. Power Sources*, 2015, **288**, 221.
19. M. A. Al-Azawi, N. Bidin, A. K. Ali and M. Bououdina, *J. Mater. Sci: Mater. Electron.*, 2015, **26**, 6276.
20. L. Bai, M. Li, K. Guo, M. Luoshan, H. F. Mehnane, L. Pei, M. Pan, L. Liao and X. Zhao, *J. Power Sources*, 2014, **272**, 1100.
21. N. Chander, P. Singh, A. F. Khan, V. Dutta and V. K. Komarala, *Thin Solid Films*, 2014, **568**, 74.
22. H. F. Zarick, O. Hurd, J. A. Webb, C. Hungerford, W. R. Erwin and R. Bardhan, *ACS Photonics*, 2014, **1**, 806.
23. Y. Lou, S. Yuan, Y. Zhao, P. Hu, Z. Wang, M. Zhang, L. Shi and D. Li, *Dalton Trans.*, 2013, **42**, 5330.
24. S. Muduli, O. Game, V. Dhas, K. Vijayamohanan, K. A. Bogle, N. Valanoor and S. B. Ogale, *Solar Energy*, 2012, **86**, 1428.
25. Y. Li, H. Wang, Q. Feng, G. Zhou and Z.-S. Wang, *Energy Environ. Sci.*, 2013, **6**, 2156.
26. L. Li, N. Wen, H. Xia, J. Li, W. Sun and L. Peng, *Sci. China Chem.*, 2015, **58**, 1501.
27. M. Jalali, R. S. Moakhar, A. Kushwaha, G. K. L. Goh, S. K. Sadrnezhaad and N. Riahi-Noori, *J. Appl. Electrochem.,* 2015, **45**, 831.
28. P. S. Musavi Gharavi and M. R. Mohammadi, *Sol. Energ. Mater. Sol. C*, 2015, **137**, 113.
29. S. D. Perrault and W. C. Chan, *J. Am. Chem. Soc*., 2009, **131**, 17042.
30. Z.-S. Wang, H. Kawauchi, T. Kashima and H. Arakawa, *Coord. Chem. Rev.*, 2004, **248**, 1381.
31. Z.-S. Wang, T. Yamaguchi, H. Sugihara and H. Arakawa, *Langmuir*, 2005, **21**, 4272.
32. H. Choi, W.T. Chen and P.V. Kamat, *ACS Nano*, 2012, **6**, 4418.
33. A. Takai and P.V. Kamat, *ACS Nano*, 2011, **5**, 7369.
34. S. Ito, P. Liska, P. Comte, R.L. Charvet, P. Pechy, U. Bach, L. Schmidt-Mende, S.M. Zakeeruddin, A. Kay, M.K. Nazeeruddin and M. Grätzel, *Chem. Commun.*, 2005, 4351.
35. L. Bai, M. Li, K. Guo, M. Luoshan, H. F. Mehnane, L. Pei, M. Pan, L. Liao and X. Zhao, *J. Power Sources*, 2014, **272**, 1100.
36. X. H. Ji, X. N. Song, J. Li, Y. B. Bai, W. S. Yang and X. G. Peng. *J. Am. Chem. Soc.*, 2007, **129**, 13939.
37. G. Plascencia-Villa, D. Torrente, M. Marucho and M. Jose-Yacaman, *Langmuir*, 2015, **31**, 3527.
38. J. G. Xu, A. R. Wilson, A. R. Rathmell, J. Howe, M. F. Chi and B. J. Wiley, *ACS Nano*, 2011, **5**, 6119.
39. H. G. Yang, C. H. Sun, S. Z. Qiao, J. Zou, G. Liu, S. C. Smith, H. M. Cheng and G. Q. Lu, *Nature*, 2008, **453**, 638.
40. S. Wang, K. Qian, X. Bi and W. Huang, *J. Phys. Chem. C*, 2009, **113**, 6505.
41. S. T. Gentry, S. J. Fredericks and R. Krchnavek, *Langmuir*, 2009, **25**, 2613.
42. T. Linnert, P. Mulvaney, A. Henglein and H. Weller, *J. Am. Chem. Soc.*, 1990, **112**, 4657.
43. S. Underwood and P. Mulvaney, *Langmuir*, 1994, **10**, 3427.
44. K. Saha, S. S. Agasti, C. Kim, X. Li and V. M. Rotello, *Chem. Rev.*, 2012, **112**, 2739.
45. P. N. Njoki, I.-I. S. Lim, D. Mott, H.-Y. Park, B. Khan, S. Mishra, R. Sujakumar, J. Luo and C.-J. Zhong, *J. Phys. Chem. C*, 2007, **111**, 14664.
46. Y. Q. He, S. P. Liu, L. Kong and Z. F. Liu, *Spectrochim. Acta A*, 2005, **61**, 2861.
47. M. L. Personick, M. R. Langille, J. Zhang, N. Harris, G. C. Schatz and C. A. Mirkin, *J. Am. Chem. Soc.*, 2011, **133**, 6170.
48. H. Li, Z. Bian, J. Zhu, Y. Huo, H. Li and Y. Lu, *J. Am. Chem. Soc.*, 2007, **129**, 4538.
49. S. W. Han, Y. Kim and K. Kim, *J. Colloid Interface Sci.*, 1998, **208**, 272.
50. W. Jiang, H. Z. Liu, L. Yin and Y. C. Ding, *J. Mater. Chem. A*, 2013, **1**, 6433.
51. D. Duche, P. Torchio, L. Escoubas, F. Monestier, J.-J. Simon, F. Flory and G. Mathian, *Sol. Energy Mater. Sol. Cells*, 2009, **93**, 1377.